Understanding single top quarks using jets

Tilman Plehn,[1] Michael Rauch,[2] and Michael Spannowsky[2]

[1]*Institut für Theoretische Physik, Universität Heidelberg, Philosophenweg 16, 69120 Heidelberg, Germany*
[2]*Institut für Theoretische Physik, Universität Karlsruhe, Wolfgang-Gaede-Str. 1, 76128 Karlsruhe, Germany*
(Received 28 July 2009; published 29 December 2009)

Top quark plus jets production at a hadron collider allows us to study the couplings of the top quark. In the standard model, two single top processes contribute to the top-jets final state. Beyond the standard model, additional direct top production can occur. All three processes probe top gauge couplings including flavor mixing. The structure of accompanying QCD jets allows us to separate the direct top signal from the QCD backgrounds as well as to disentangle the three top plus jets production mechanisms orthogonally to the usual bottom tags.

I. INTRODUCTION

Experimental results from flavor physics and electroweak precision measurements have long established the standard model pattern of flavor and CP violation. The only sources of flavor and CP violation are the Yukawa couplings, and the one essentially unknown parameter is the relative coupling strength of the heavy third-generation quark to the W boson, i.e. the Cabibbo-Kobayashi-Maskawa (CKM) mixing angle V_{tb} [1]. Its knowledge is crucial to establish the unitarity of the CKM mixing matrix in the standard model. Because the SU(3) symmetry of QCD does not see electroweak charges, this coupling cannot be determined in QCD-mediated top pair production. Instead, we rely on the electroweak production process for a single top quark in association with a quark jet to measure this parameter of the standard model.

The problem of modern particle physics is that while on the one hand we have good reasons to expect that we will see a nontrivial ultraviolet completion of the standard model at the TeV scale, we do not know where in such an extended model this particular flavor structure originates from. One of the standard candidates for such new physics at the TeV scale with all of its benefits from a dark matter candidate and stabilized Higgs mass to a valid grand unified theory is the minimal supersymmetric standard model (MSSM) [2]. Mainly in the soft-breaking terms in the MSSM Lagrangian there are multiple sources of flavor and CP violation which naturally predict observable effects, including flavor-changing neutral currents. Assuming only one set of supersymmetric partner states, we can implement the experimental constraints by postulating a symmetry dubbed minimal flavor violation. This implies that there will still be no sources of flavor violation other than the Yukawa couplings, the spurions of flavor symmetry breaking [3]. An interesting alternative might be the promotion of the gauge sector to $N = 2$ supersymmetry, leading to Dirac fermion partners of the standard model gauge bosons and additional scalar particles, all clearly visible at the LHC [4,5].

In this paper, we instead focus on the more subtle effects of an approximate minimal flavor violation symmetry. Focusing on the quark/squark sector, minimal flavor violation forces the soft squark masses to be almost diagonal in flavor space and the scalar trilinear A terms—for example, describing squark-squark-Higgs interactions—to be proportional to the Yukawa couplings. Corrections consistent with the standard model flavor symmetry are induced by higher powers in the Yukawa couplings.

Since we cannot derive minimal flavor violation from first principles, we need to measure if and by how much it is broken. In the down-quark sector, squarks contribute to K- and B-physics observables via squark-gluino loops mediated by the strong coupling constant α_s, which gives us powerful tests of minimal flavor violation. In contrast, in the up-quark sector, such one-loop effects are proportional to the weak coupling α or the Yukawa couplings and much harder to measure. The first third- and second third-generation mixing between the $\tilde{u}_R$ and $\tilde{c}_R$ with $\tilde{t}_L$ squarks is essentially invisible for kaon, charm, and B experiments [6,7]. Integrating out the heavy supersymmetric particles, such loop contributions lead to flavor-violating quark couplings to standard model gauge bosons, for example, a u-t-g or c-t-g vertex [8]. At the LHC, processes involving valence quarks are generally more interesting, so we will focus on the u-t-g vertex, but its second generation counterpart can of course be treated the same way.

The search for this largely unconstrained effective coupling is linked with the measurement of V_{tb} through the relevant LHC processes. While the effective gluon vertex leads to the direct production of an isolated top quark, single top production is accompanied by a quark jet. However, at the LHC we know that the radiation of additional quark and gluon jets from the incoming quarks is ubiquitous. Therefore, the question becomes, how can we tell apart electroweak CKM effects in single top production (and its two production mechanisms) and strong effects from nonminimal new physics in direct top production, all including top quark decays as well as realistic QCD effects

and backgrounds? Recently, a model independent analysis has been done for the direct top production channel [9].

II. DIRECT TOPS AND JETS

In spite of the fact that there are many flavor observables constraining squark mixing beyond minimal flavor violation, there are two entries in the squark mass matrices which are still largely unconstrained. Even though we actually use the diagonalized squark mass matrix, it is instructive to discuss the results in terms of dimensionless mass insertions $\delta_{AB,ij}^q = \Delta_{AB,ij}^q / \bar{m}^2$ (for the squark handedness $A, B = L, R$, the generation indices $i, j = 1 \cdots 3$, and the weak isospin $q = u, d$). The $\Delta_{AB,ij}^q$ are the relevant off-diagonal entries, and $\bar{m}^2 = m_{AA,ii} m_{BB,jj}$ is the corresponding mean diagonal entry in the squark mass matrix.

Because we are not interested in the strongly constrained down-type mixings δ^d and we focus on left-right mixing only, we denote

$$\delta_{ij} \equiv \delta_{LR,ij}^u. \tag{1}$$

The unconstrained left-right mixing terms are the off-diagonal δ_{31} between $\tilde{u}_R$ and $\tilde{t}_L$ and the diagonal δ_{33} [7,10]. The left-right swapped δ_{13} instead mixes $\tilde{u}_L$ and $\tilde{t}_R$. It is constrained by $b \to d$ transitions [11] and Δm_d in $\bar{B}_d - B_d$ mixing [12]. The reason why the bounds on δ_{13} are strong and those on δ_{31} hardly exist is the chargino-top loop: if the chargino is a mix of the wino and the Higgsino, the latter will have a large Yukawa coupling to the external bottom. The $\tilde{u}$ instead couples to the wino content of the chargino, which forces it to be left handed $\tilde{u}_L$. This δ_{13} constraint can only be relaxed by heavy squarks.

Assuming minimal flavor violation, the generation-diagonal entry Δ_{33} is of the general form $m_t(A_t - \mu/\tan\beta)$ and does not need to be small. As a matter of fact, it can lead to a large splitting of the two stop masses and ameliorates the little hierarchy problem, so we do not expect it to be small either. It is currently only constrained via the lower limit on the light Higgs mass and can be measured either in stop mixing or in the minimal supersymmetric Higgs sector [13].

The generation mixing entry δ_{31} mixes $\tilde{u}_R$ and $\tilde{t}_L$ and at one-loop, induces the flavor-changing chromomagnetic operator [14]

$$m_{\tilde{g}} \frac{g_s}{16\pi^2} \bar{t}_{L,\alpha} \sigma_{\mu\nu} u_{R,\beta} T_{\alpha\beta}^a G_a^{\mu\nu} + \text{H.c.} \tag{2}$$

via a squark-gluino loop. As shown on the left Fig. 1, this operator implies direct top production at hadron colliders $pp \to t \to bW_\ell^+$, with a leptonic W decay to avoid an undetectable purely hadronic final state. The corresponding partonic cross section is typically suppressed by the heavy gluino mass in the loop and therefore proportional to

$$\sigma(ug \to t) \propto \frac{|\delta_{31}|^2 |\delta_{33}|^2}{m_{\tilde{g}}^2}. \tag{3}$$

The second diagram in Fig. 1 contributes proportionally to $|\delta_{13}|^2$, which is negligible after fulfilling all-flavor constraints. Because of the absolute values squared, they are invariant under complex phases of the squark mixing parameters. This process, to our knowledge, is the only way to measure the otherwise unaccessible δ_{31} in the era of LHC and super-B factories.

Usually, the MSSM parameter space beyond minimal flavor violation is huge, and physical processes typically involve many possible contributions which are free to cancel each other. In contrast, direct top production is a strongly interacting process and depends only on the masses $m_{\tilde{g}}$ and $m_{\tilde{t}_1}$ and the squark mixing parameters $\delta_{33} \sim A_t$, δ_{31} and δ_{13}. For small values of $\tan\beta$, we have to include $\mu/\tan\beta$ in the expression for δ_{33}. For our numerical study, we use the snowmass points and slopes 2 [15] inspired reference point with the grand unified theory-scale masses $m_0 = 1450$ GeV, $m_{1/2} = 300$ GeV, and $A_0 = 0$. The Higgs sector is characterized by $\tan\beta = 10$ and $\mu > 0$. The relevant weak-scale masses for our process are

$$\tan\beta = 9.6, \qquad \mu = 386 \text{ GeV},$$
$$M_{\tilde{\chi}_1^0} = 125 \text{ GeV}, \qquad M_{\tilde{g}} = 350 \text{ GeV}, \tag{4}$$
$$m_{\tilde{U}_{L,11}} = m_{\tilde{U}_{L,22}} = 1538 \text{ GeV}, \qquad m_{\tilde{U}_{L,33}} = 1279 \text{ GeV},$$
$$m_{\tilde{U}_{R,11}} = m_{\tilde{U}_{R,22}} = 1534 \text{ GeV}, \qquad m_{\tilde{U}_{R,33}} = 956 \text{ GeV}.$$

This gives us a light (mostly) stop mass of 955 GeV and a light Higgs mass of 117 GeV. The lightest neutralino is a viable dark matter candidate. For the calculation of the direct top production rate at this point we use FEYNARTS, FORMCALC [16], LOOPTOOLS [17], and HADCALC [18]. We
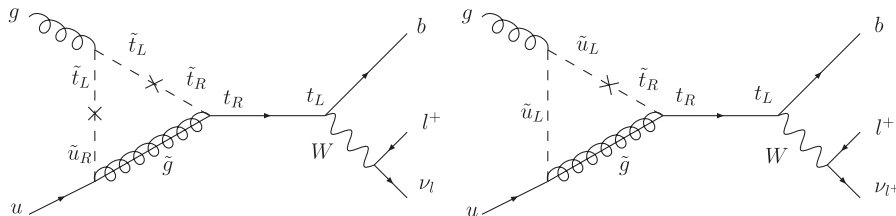

FIG. 1. Sample Feynman diagrams for SUSY-induced direct top production. The crosses indicate left-right mass insertions which can mix first- and third-generation up squarks.

include all supersymmetric QCD and electroweak contributions.

There are four major backgrounds for direct top production $ug \to bW^+$ (see Fig. 2) with a charge identified lepton from the W decay and a tagged bottom jet with a tagging probability of 50% and a mistagging probability of 1%:

$$
\begin{aligned}
ug &\to bW^+ && \text{irreducible and CKM suppressed,} \\
ug &\to dW^+ && \text{fake bottom tag,} \\
\bar{d}g &\to \bar{c}W^+ && \text{fake bottom tag,} \\
u\bar{d} &\to b\bar{b}W^+ && \text{gluon splitting to two bottoms.}
\end{aligned}
\tag{5}
$$

Of the three W plus one jet backgrounds, the irreducible combination is suppressed with respect to the mistagging background by roughly 2 orders of magnitude. Similarly, the more likely mistag of a charm requires a $\bar{d}g$ initial state and should be at a maximum of the same order as the valence-quark induced $ug \to dW^+$ process. Most importantly, the kinematic distributions of the three are very similar, so we expect all three to vanish as a roughly constant fraction of the leading $ug \to dW^+$ background.

The two-bottoms background process can become dangerous when the two bottom jets are close enough to look like one bottom jet from gluon splitting. If we require the two bottom jets to be close ($\Delta R_{bb} < 0.6$), the resulting $W^+ b\bar{b}$ rate is of the same order as the subleading bW^+ production, which again means that in the following discussion, we will focus on the mistagged $ug \to d_bW^+$ background.

All of the background and the signal pass the acceptance (and triggering) cuts

$$
\begin{aligned}
p_{T_b} &> 20 \text{ GeV,} & p_{T_\ell} &> 15 \text{ GeV,} \\
|\eta_b|, |\eta_\ell| &< 2.5, & \Delta R_{b\ell} &> 0.4
\end{aligned}
\tag{6}
$$

without a major reduction. Note that we apply bottom acceptance cuts to the mistagged light jet in the background, so at this level there will not be any light-flavor jets in the analysis.

There are two key distributions to separate direct top production from the continuum backgrounds, shown in Fig. 3: due to the signal kinematics, the transverse momentum of the bottom jet is strongly peaked around $p_{T_b} \sim (m_t^2 - m_W^2)/(2m_t) \simeq 67.5$ GeV, even including detector effects. For the signal, the partonic center of mass energy $\sqrt{\hat{s}}$ should also peak around the top mass. We compute the unmeasured longitudinal neutrino momentum from the mass shell condition $m_{l\nu} = m_W$. We resolve the remaining two-fold ambiguity by choosing the better top mass reconstruction [14]. We exploit these kinematic features by requiring

$$
\begin{aligned}
55 \text{ GeV} &< p_{T_b} < 80 \text{ GeV,} \\
165 \text{ GeV} &< \sqrt{\hat{s}_{\text{rec}}} < 185 \text{ GeV.}
\end{aligned}
\tag{7}
$$

As shown in Table I, the statistical significance after cutting on the kinematic features of the signal is not sufficient to extract single top production at the LHC, even though the Gaussian significance for 60 fb^{-1} of data looks promising. Theory and other systematic errors require a reasonable value of at least $S/B \gtrsim 1/10$ for such a counting experiment, which means that we have to search for addi-
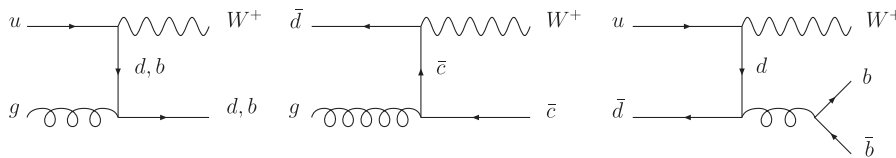

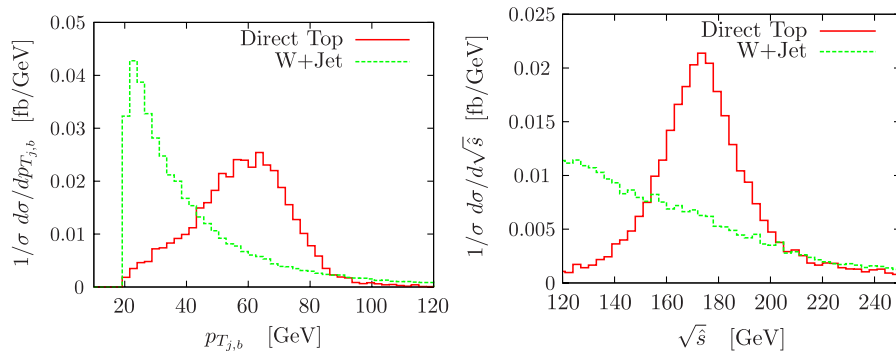FIG. 2.   Major backgrounds for the direct top production.

FIG. 3 (color online).   Normalized distributions for direct top production and the main background $pp \to \nu\ell^+ + $ jets, after acceptance cuts. These distributions (and only these) are generated without QCD jet radiation but include momentum smearing to account for detector effects.

TABLE I.　Signal and background rates for direct top production after acceptance cuts [Eq. (6)], resonance cuts [Eq. (7)], existing additional QCD jets [Eq. (8)], and finally correlation cuts on this QCD jet activity [Eq. (9)]. The statistical significances assume 60 fb^{-1} of luminosity at 14 TeV. For the merged sample, we only consider the leading background.

	σ_S	σ_{Wj}	σ_{Wb}	S/B	$S/\sqrt{B}$
After acceptance cuts	50 fb	12944 fb	105 fb	1/260	3.4
After resonance cuts	13.2 fb	496 fb	4.4 fb	1/38	4.6
Requiring second jet	7.2 fb	160 fb		1/22	4.4
After jets cuts	5.0 fb	48 fb		1/9.6	5.6

tional ways to extract direct top production out of the QCD background.

A distinguishing feature of direct top production, which has nothing to do with the decay kinematics, is that coming from a ug initial state, the produced top quark will be boosted longitudinally following the direction of the valence quark. We can follow this behavior by noticing that for the signal, the lepton and, in particular, the bottom quark are moving into the forward direction, peaked around pseudorapidities of two. In contrast, the QCD background behaves like Drell-Yan W production with one parton splitting in the initial state, where the W boson, as well as the lepton, are central. Interestingly enough, the radiated mistagged jet above our p_T threshold is also fairly central. The problem with this general kinematic feature is that it is not strong enough to allow for an efficient cut in

our analysis. This changes once we include further QCD jet radiation.

To simulate the radiation of QCD jets beyond the leading jet, we employ the MLM matching scheme with the Pythia shower, as implemented in MADEVENT [19–21]. This allows us to consistently add $pp \to t +$ jets samples with an arbitrary number of additional jets [22,23]. For large transverse momenta, these jets will be correctly described by the hard matrix element, and for small transverse momenta, also correctly by the parton shower. While the main motivation for such jet merging simulations are, for example, $W +$ jets samples as backgrounds to Higgs and new-physics searches, the same method allows us to simulate jet radiation accompanying heavy states at the LHC and exploit these patterns to improve the signal extraction [5,24].

First, we ask for additional jets from QCD radiation, which have to pass the staggered jet acceptance cuts

$$p_{T_j} > 30, 30, 20 \text{ GeV}, \qquad |\eta_j| < 2.5. \qquad (8)$$

Including effects of the underlying event is beyond the aim of this study, which also means that details of the jet algorithm should not affect our result significantly. One of these three jets should be the bottom jet from the top decay. Usually, the top decay jet will be the hardest, maybe the second hardest jet. This means that one of the two 30 GeV jets will, in addition, have to pass the top resonance cut of $p_{T_b} > 55$ GeV as listed in Eq. (7). This
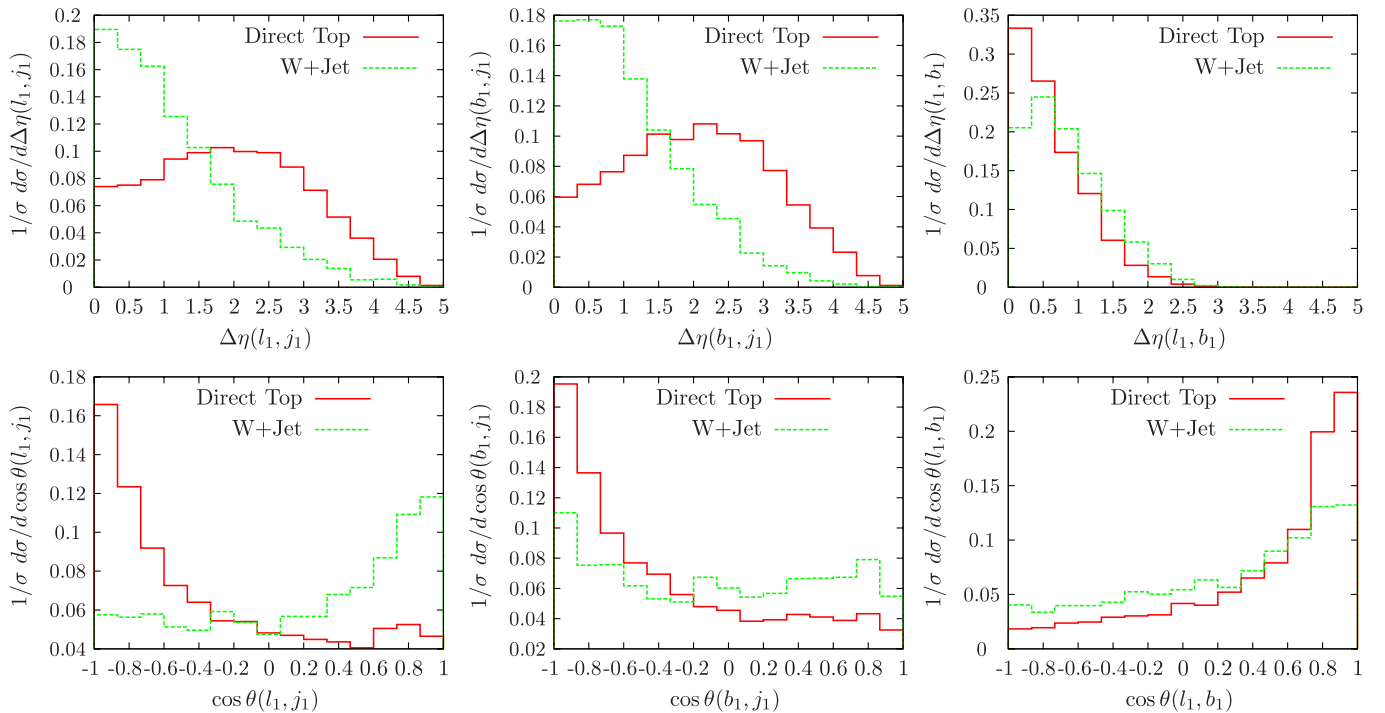

FIG. 4 (color online).　Correlations of the first radiated QCD jet with the particles from the hard process for the direct top signal and the QCD background, after applying all acceptance and the top resonance cuts. We show the (similar) behavior of the pseudorapidity difference and the full opening angle.
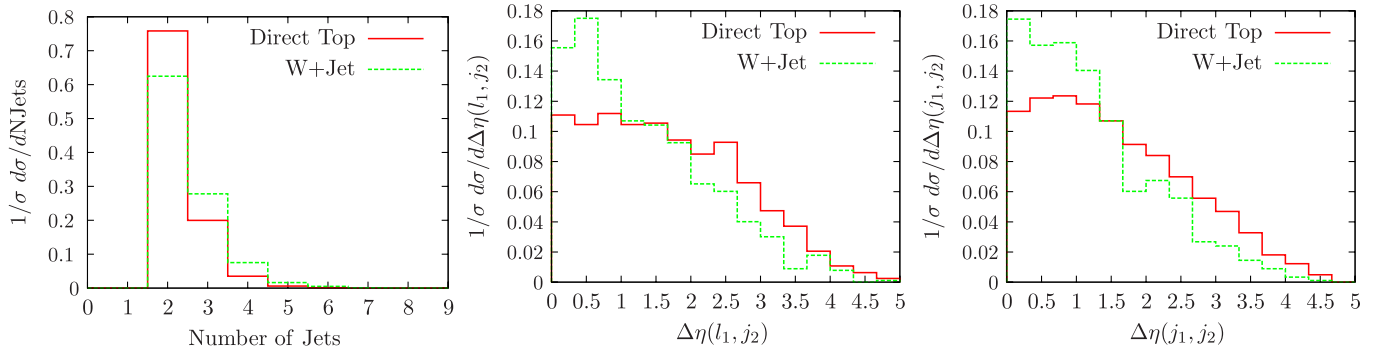
FIG. 5 (color online). Correlations of the second radiated QCD jet, corresponding to Fig. 4.

feature, as well as our aim to be not too dependent on the details of the jet merging simulation, motivates us, even for the light-flavor jets, to consider only maximum pseudorapidities of 2.5. In this aspect, a more dedicated analysis of the bottom tag could significantly improve the signal efficiency and hence the Gaussian significance. While 20 GeV for the third jet sounds very small, this analysis is also meant to show the impact that the analysis of the QCD jet activity can have on new-physics searches, so we decide to keep it as low as possible. Depending on the structure of the measured underlying event, this threshold might have to be increased eventually.

We show the improvement of the direct top analysis just through requiring the existence of two jets in Table I. The higher apparent probability to radiate one additional jet from the signal process is related to a larger number of soft jets for the continuum background, as we will see later. This is due to the continuum structure of the background diagrams without a hardly radiating resonant top quark and the fact that the mistagged bottom is actually a massless jet and more likely to split collinearly.

Just based on our argument above and on color factors, in the signal case the radiation off the incoming gluon will dominate the radiation pattern. This means that the top quark and the leading QCD jet fly into opposite directions. We can see this behavior in the pseudorapidity distributions as well as in the opening angle distributions in Fig. 4: the first radiated jet for the signal is indeed widely separated from the lepton as well as the bottom jet, i.e. from the top quark. In contrast, the continuum QCD background radiates jets over a wide pseudorapidity range, bounded only by the maximum pseudorapidity of 2.5. Because the lepton is central, this means that the pseudorapidity difference between the lepton and the first jet has to drop off fast once we go to pseudorapidities of order two. The same is true for the pseudorapidity difference of the first two radiated jets, one of which is falsely tagged as a bottom jet: if both are reasonably central, their pseudorapidity difference is rarely going to exceed values of 2.5.

We can now cut on these well distinguishable jet distributions to separate signal and background. Symmetrically, we constrain the two pseudorapidity differences to be

$$\Delta\eta_{b_1,j_1} > 1, \qquad \Delta\eta_{\ell,j_1} > 1 \qquad (9)$$

and show the results in Table I. While these cuts do not improve the statistical significance much beyond the top reconstruction cuts, they bring down S/B to a manageable level. Refining these jet cuts, we can further improve S/B, but at the expense of the number of signal events left in the analysis.

Just out of curiosity, we can check what happens once we include a second QCD jet (i.e. altogether three jets) in our analysis. Obviously, this is not suitable for the full analysis, but it could give interesting information for those signal and background events in which we see such an additional jet. We show the distribution of the number of jets in the first panel of Fig. 5. In the jet distributions, the general pattern of the first QCD jet is still present—largely, because it is based on the boosted nature of the top quark in the hard signal process. In Fig. 5, we see a similar correlation between the second QCD jet and the lepton as we see
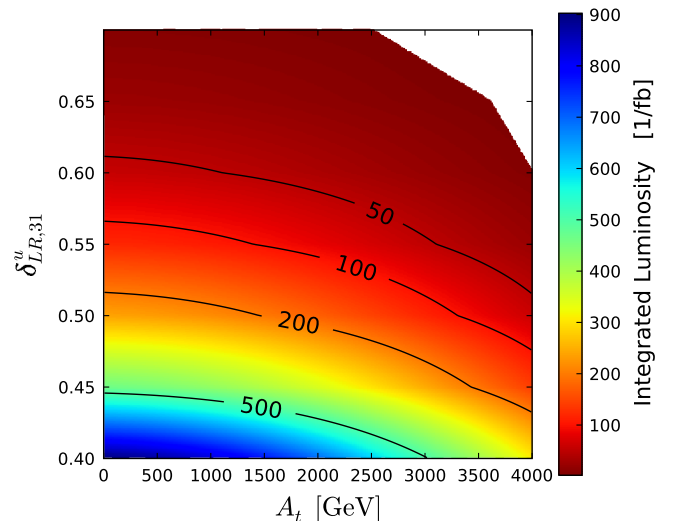

FIG. 6 (color online). Necessary integrated luminosity for 95% C.L. signal, assuming Gaussian statistics with $S/\sqrt{B}$. The white area in the upper right corner is already excluded by experimental squark searches. We adopt a squark mass bound of $m_{\tilde{q}} > 95.7$ GeV.

for the first jet. The pseudorapidity difference between the two QCD jets is also more strongly peaked in the generally central continuum background.

Based on Table I, we can compute the 95% confidence level coverage of direct top production in the $\delta_{31} - \delta_{33}$ plane. In Fig. 6, we see that with a mild dependence on $A_t \sim \delta_{33}\sqrt{m_{\tilde{t},L}^2 m_{\tilde{t},R}^2}/\langle H^u \rangle$, the LHC will be able to rule out nonminimal flavor violation through the mass matrix entry above $\delta_{31} \gtrsim 0.5$, dependent on the acquired luminosity.

III. SINGLE TOPS AND JETS

At the LHC, more signal processes contribute to the one-top-plus-jets final state [25]. The two irreducible cousins of direct top production with jet radiation are the single top production channels shown in Fig. 7: one of them proceeds via a spacelike t-channel W boson [26,27] and the other through a timelike s-channel W boson [28]. We do not consider the associated tW production [29] in this analysis, because its final state is significantly different and neither related to QCD not irreducible from direct top production. Encouraged by the signal vs background direct top analysis in the last section, we can ask if more generally the structure of QCD jet radiation [30] will allow us to distinguish these three single top and direct top production mechanisms and tell apart the responsible coupling in or beyond the standard model [31].

Usually, the three direct/single top production channels are distinguished using bottom tags, where aside from the top decay products, the t-channel process involves a forward bottom jet, while the s-channel process is accompanied by a central bottom jet and direct to production does not involve additional bottom jets at all [32]. Already for the single top channels alone, identifying the different QCD features first and cross-checking for bottom flavor later might allow us to improve the V_{tb} measurement in and beyond the standard model. From the appearance of the initial-state bottom quark in the t-channel process, we know that there should exist a (collinear) forward bottom jet in the final state. However, tagging such a forward bottom comes at a large expense due to the rapidity range of flavor tagging, even as compared to simply observing it as a jet. At the same time, studying the forward b jet in the t-channel process without tagging it from the beginning also improves our sensitivity to flavor or family changing q-t-W couplings enhanced by the valence-quark parton densities [31].

We simulate direct top production as well as the two single top production processes including two additional hard QCD jets. Additional QCD jets can arise from the parton shower and are described over their entire phase space by MLM jet merging implemented in MADEVENT [19,20,33]. We subtract all $t\bar{t}$ events appearing as part of the merged sample. Because at this stage we are not suggesting a dedicated analysis, we first assume we know which of the jets are bottom jets and which are light-flavor jets. For all of them, we require the staggered acceptance cuts

$$p_{T_j} > 30, 30, 20, 20, 20 \cdots \text{ GeV}, \qquad |\eta_j| < 2.5. \quad (10)$$

The pseudorapidity range is the same for bottom and light-flavor jets and avoids distinguishing bottoms and light-flavor jets. This way, we can later apply our analysis to all-flavor jets. To ensure that these signal events pass the triggers, we request one lepton from the top decay with

$$p_{T_\ell} > 15 \text{ GeV}, \qquad |\eta_\ell| < 2.5, \qquad \Delta R_{j\ell} > 0.4. \quad (11)$$

Without showing all the distributions, we know what to expect for the p_T spectrum of the accompanying jets in the three processes: in the t-channel process, there will be one hard central jet balancing the top quark and a second forward b jet from the gluon splitting. Tagging this forward bottom jet might or might not be useful, dependent, for example, on the optimization of the signal vs background analysis with respect to S/B or $S/\sqrt{B}$ [34]. This forward bottom jet will be collinearly divergent, regularized by the bottom mass, i.e. down to transverse momenta of $p_T < 10$ GeV, its p_T spectrum will diverge. The QCD jet, which balances the top, peaks at transverse momenta around 40–50 GeV, almost as high as the bottom jet from the top decay (with its Jacobian peak around 65 GeV). This we can understand when we consider this process as one-sided weak boson fusion.

In the s channel, the flavor structure of the standard model enforces a second bottom jet from the off-shell W decay. This jet plays a similar balancing role as the light-flavor jet in the t-channel process. We now we see two competing hard bottom jets of comparable p_T, both peaking around 40–80 GeV.

Direct top production in contrast does not predict any additional hard jets in the detector. Because it involves a flavor-changing production vertex, there should be no additional bottom jets, and the light-flavor jets will follow the typical initial-state radiation pattern.
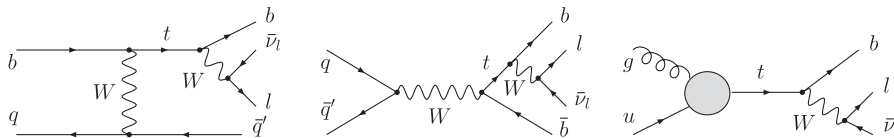

FIG. 7. Sample Feynman diagrams for the three single/direct top production mechanisms at hadron colliders. For direct top production, we represent the effective ugt vertex with a solid circle.

To describe the angular correlations of the final state [35] including QCD jets in more detail, we consider the observable $\cos\theta^*(P_1, P_2)$ between the two particles P_1 and P_2 (or their respective three momenta $\vec{p}_{1,2}$). It parametrizes the angle between $\vec{p}_1$ in the combined $P_1 + P_2$ rest frame and $(\vec{p}_1 + \vec{p}_2)$ in the lab frame. It is not symmetric in its arguments. If the two particles are back to back and $|\vec{p}_1| > |\vec{p}_2|$,

it approaches $\cos\theta^* = 1$; whereas, for $|\vec{p}_1| < |\vec{p}_2|$, it becomes -1. In between, it vanishes in the case where $\vec{p}_1$ in the center of mass frame is orthogonal to the lab frame movement of this center of mass.

We confirm this behavior in the first row of Fig. 8. For t-channel single top production, the hardest light-flavor jet balances the top, so the lepton is most likely back to back
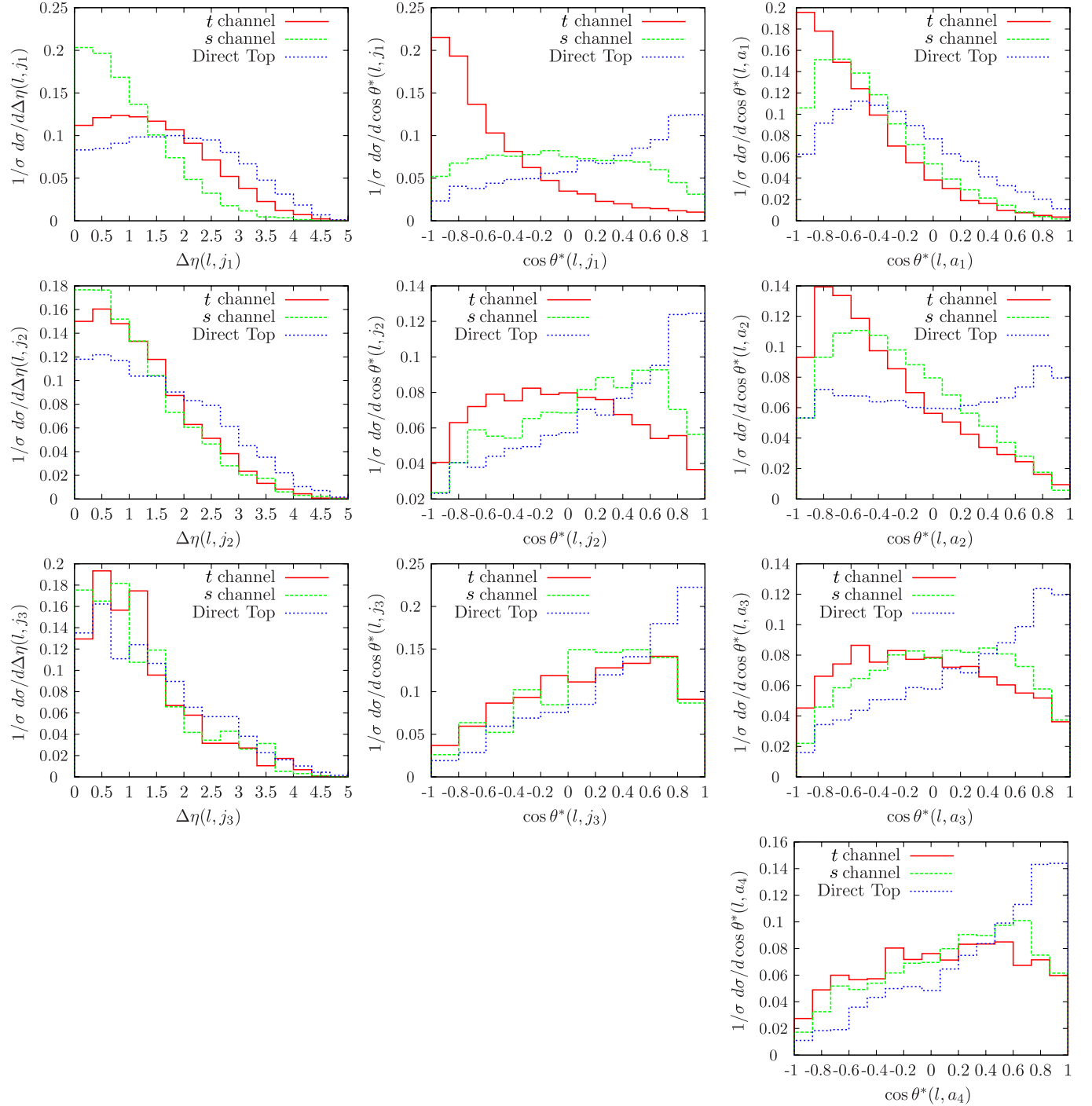

FIG. 8 (color online).   QCD jet-lepton correlations for single and direct top production. We show the pseudorapidity difference as well as the $\cos\theta^*$ dependence as discussed in the text. The label a represents all-flavor jets which might be bottom jets (b) or light-flavor jets (j).

with the hardest jet. Because it balances the heavy top, the leading jet is harder than the lepton and the $\cos\theta^*_{\ell j_1}$ distribution peaks at -1. For the s channel, the decay lepton will be central, as the first QCD jet will be. Except for the azimuthal angle, we expect no back-to-back configuration, which gives us $\cos\theta^*$ values flat around zero. In direct top production, the first jet is radiated at high rapidity. Because of the color factor, it most likely comes from the gluon, which means it will be collinear as well as soft. The top is boosted against the incoming gluon and with it, the decay lepton. This means that the lepton and the first QCD jet is back to back, and the hard decay lepton will be more energetic than the soft collinear jet. The $\cos\theta^*$ distribution will then peak around $+1$.

Considering further jets in t-channel single top production, the lower energy of subsequent jet radiation washes out the $\cos\theta^*$ behavior. This is due to the role of the energy hierarchy with respect to the lepton in this observable. Once we arrive at jet number three, all we see is a general parton shower jet radiation, slightly forward but uncorrelated with the top decay products. For the direct top channel, the pattern of the second jet resembles the first, because the radiation off the incoming gluon will still dominate. Similarly, additional jets accompanying s-channel top production will become slightly more forward and hence more likely to move towards larger $|\cos\theta^*|$ values, but without an exploitable structure.

Following our original motivation, what is most interesting is angular correlation of light-flavor and bottom jets without assuming a b tag. In the right column of Fig. 8, we

see that for t-channel single top production, the hardest all-flavor jet indeed balances the top quark, i.e. it is not bottom flavored. The second hardest jet then comes from the top decay, which we can check by comparing its features with the bottom correlations shown in Fig. 9. The third and forth jets both arise from parton splitting and do not have distinct correlations with the top decay products—being bottom flavored or not. Checking their p_T distribution, we can confirm that they simultaneously drop off fast at values above 40 GeV.

For s-channel single top production, both leading all-flavor jets have little to do with the $\cos\theta^*_{\ell j_1}$ distribution, which means they are the two bottom jets from the hard process. Again, we confirm this behavior in Fig. 9. In this figure, we also see that essentially all bottom jets prefer values of $\cos\theta^*_{\ell b} \rightarrow -1$, which means the bottom jets balance the lepton direction and the bottom energy lies above the lepton energies. This is simply an effect of the intermediate W decay step which softens the W decay product as compared to the bottom jet.

For direct top production, the hardest jet is usually the bottom decay jet. In addition, we expect no more bottom jets, so the distributions of j_n match those of a_{n+1}. Because the argument of the color factor preferring radiation off the incoming gluon combined with the boosted center of mass frame holds in general, subsequent jets show a similar preference for $\cos\theta^* \rightarrow 1$.

Beyond the individual jet-lepton correlations, we can also study the correlations between the different all-flavor
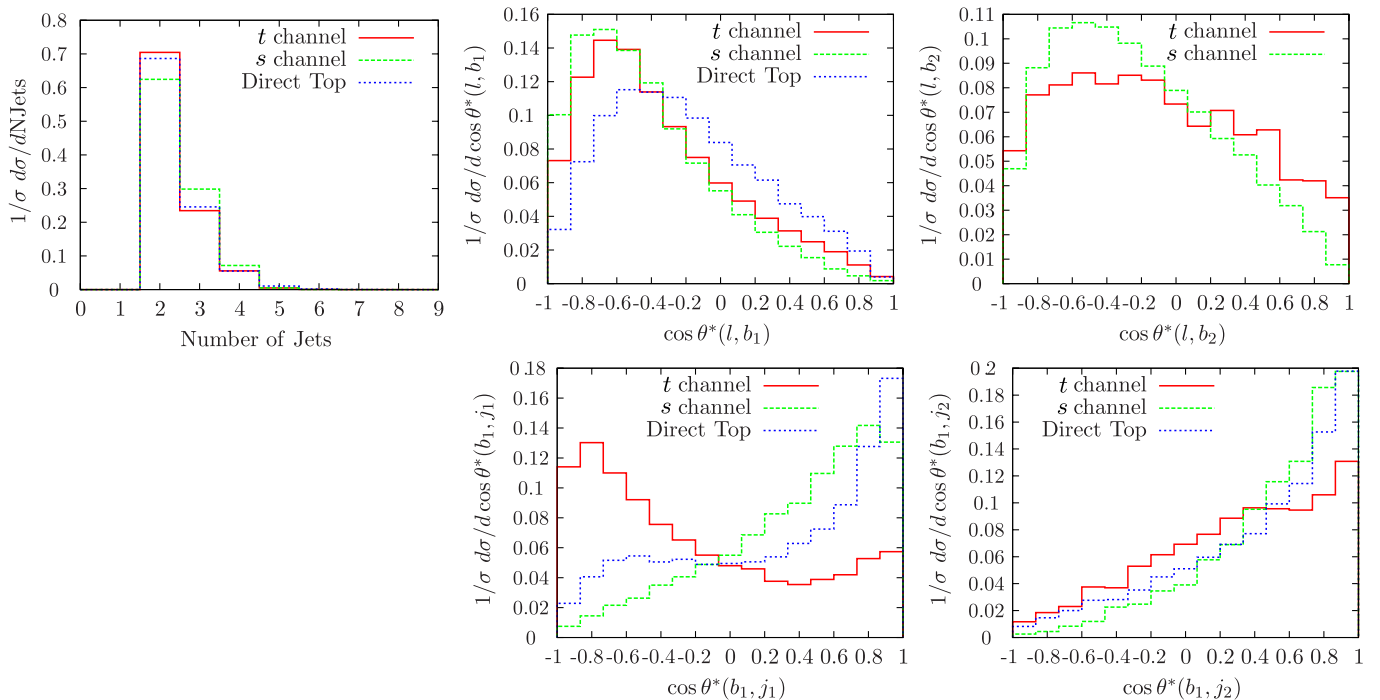

FIG. 9 (color online).   Correlations of the up to two bottom jets with the lepton from the top decay, corresponding to Fig. 8. We also show the correlation of the leading bottom jet with the first two light-flavor jets.
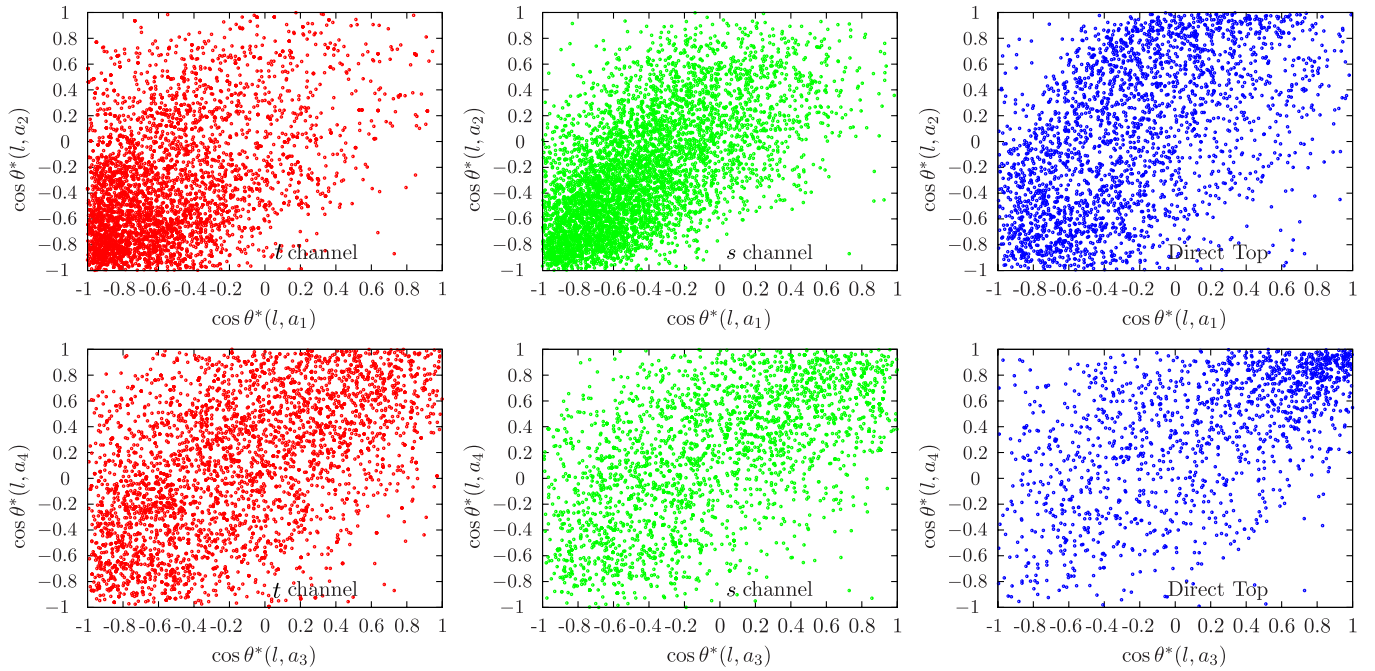
FIG. 10 (color online). Sample angular correlations between the $\cos\theta^*_{\ell a}$ for all-flavor jets. From left to right, we show t-channel single top production, s-channel single top production, and direct top production.

jets. In Fig. 10, we should sample distributions of this kind for the three production processes under consideration.

For the t-channel process, we already know that the two leading jets, one light-flavor and one the bottom decay jet, both reside at small values of $\cos\theta^*_{\ell a}$. The third and fourth jet, again one bottom and one light-flavor, do not have a strong preference for large values of $|\cos\theta^*_{\ell a}|$, but in contrast to the leading two jets, they show a correlation with each other, based on the general radiation pattern.

In the s-channel process, the two leading jets are the two bottom jets. They are correlated and prefer small values of $\cos\theta^*_{\ell a_j}$, dependent mostly on the lepton energy. For the next two jets, the correlations are considerably weaker, and from Fig. 8 we already know not to expect much information in their $\cos\theta^*_{\ell a}$ distributions.

Direct top production produces a hard bottom jet with a slight preference towards $\cos\theta^* \rightarrow -1$. Aside from that, the universal jet radiation structure shows a diagonal correlation with the slightly favored region $\cos\theta^* \rightarrow 1$, becoming much more prominent for the two subleading jets.

IV. OUTLOOK

In this paper, we have shown how we can exploit the QCD jet activity to extract direct top production from the QCD background and to tell apart t-channel single top production, s-channel single top production, and direct top production.

Direct top production is the only way to observe or constrain the supersymmetric flavor-violating squark mass entry $\delta^u_{LR,31}$ in the near future. It is mediated by the flavor-changing neutral current u-t-g interaction and has to

be extracted from W + jets backgrounds with a light-flavor jet mistagged as a bottom. While kinematic cuts based on the top resonance structure of the matrix element are not sufficient to produce a promising signal-to-background ratio S/B, we find that additional cuts on the jet correlation from QCD radiation improve this ratio enough to allow for a meaningful LHC analysis.

The same kind of QCD jet correlations with the top decay lepton allow us to distinguish (normalized) samples of t-channel single top production, s-channel single top production, and direct top production. All three channels are irreducible if we consider searches for one top quark plus jets. Our distinction is purely based on angular correlations and serves as an orthogonal test to possible bottom tags. In single top searches, applying explicit bottom tags only later in the analysis allows us to make use of the parton density enhancement when looking for flavor-changing top couplings. Both methods combined should be able to unambiguously determine the third-generation flavor structure of the standard model, including the CKM mixing element V_{tb} as well as new-physics effects.

[1] C. Amsler *et al.* (Particle Data Group), Phys. Lett. B **667**, 1 (2008); F. Abe *et al.* (CDF Collaboration), Phys. Rev. Lett. **74**, 2626 (1995); S. Abachi *et al.* (D0 Collaboration), Phys. Rev. Lett. **74**, 2632 (1995); V. M. Abazov *et al.* (D0 Collaboration), Phys. Rev. D **78**, 012005 (2008).

[2] H. E. Haber and G. L. Kane, Phys. Rep. **117**, 75 (1985).

[3] G. D'Ambrosio, G. F. Giudice, G. Isidori, and A. Strumia, Nucl. Phys. **B645**, 155 (2002); B. C. Allanach, G. Hiller, D. R. T. Jones, and P. Slavich, J. High Energy Phys. 04 (2009) 088.

[4] G. D. Kribs, E. Poppitz, and N. Weiner, Phys. Rev. D **78**, 055010 (2008); G. D. Kribs, A. Martin, and T. S. Roy, J. High Energy Phys. 06 (2009) 042.

[5] T. Plehn and T. M. P. Tait, J. Phys. G **36**, 075001 (2009).

[6] L. J. Hall, V. A. Kostelecky, and S. Raby, Nucl. Phys. **B267**, 415 (1986); J. S. Hagelin, S. Kelley, and T. Tanaka, Nucl. Phys. **B415**, 293 (1994); F. Gabbiani, E. Gabrielli, A. Masiero, and L. Silvestrini, Nucl. Phys. **B477**, 321 (1996); M. Misiak, S. Pokorski, and J. Rosiek, Adv. Ser. Dir. High Energy Phys. **15**, 795 (1998); M. Ciuchini, E. Franco, A. Masiero, and L. Silvestrini, Phys. Rev. D **67**, 075016 (2003); **68**, 079901(E) (2003); A. Bartl, K. Hidaka, K. Hohenwarter-Sodek, T. Kernreiter, W. Majerotto, and W. Porod, Phys. Lett. B **679**, 260 (2009).

[7] S. Dittmaier, G. Hiller, T. Plehn, and M. Spannowsky, Phys. Rev. D **77**, 115001 (2008).

[8] T. M. P. Tait and C. P. Yuan, Phys. Rev. D **55**, 7300 (1997); J. Cao, G. Eilam, K. i. Hikasa, and J. M. Yang, Phys. Rev. D **74**, 031701 (2006); J. Guasch, W. Hollik, S. Penaranda, and J. Sola, Nucl. Phys. B, Proc. Suppl. **157**, 152 (2006); J. J. Cao, G. Eilam, M. Frank, K. Hikasa, G. L. Liu, I. Turan, and J. M. Yang, Phys. Rev. D **75**, 075021 (2007).

[9] T. Aaltonen *et al.* (CDF Collaboration), Phys. Rev. Lett. **102**, 151801 (2009).

[10] J. A. Casas and S. Dimopoulos, Phys. Lett. B **387**, 107 (1996).

[11] K. Abe *et al.*, Phys. Rev. Lett. **96**, 221601 (2006); B. Aubert *et al.* (*BABAR* Collaboration), Phys. Rev. Lett. **98**, 151802 (2007).

[12] E. Barberio *et al.* (Heavy Flavor Averaging Group), arXiv:hep-ex/0603003, http://www.slac.stanford.edu/xorg/hfag.

[13] R. Lafaye, T. Plehn, M. Rauch, and D. Zerwas, Eur. Phys. J. C **54**, 617 (2008); R. Lafaye, T. Plehn, M. Rauch, D. Zerwas, and M. Duhrssen, J. High Energy Phys. 08 (2009) 009.

[14] E. Malkawi and T. M. P. Tait, Phys. Rev. D **54**, 5758 (1996); M. Hosch, K. Whisnant, and B. L. Young, Phys. Rev. D **56**, 5725 (1997); T. Han, M. Hosch, K. Whisnant, B. L. Young, and X. Zhang, Phys. Rev. D **58**, 073008 (1998); A. Belyaev, arXiv:hep-ph/0007058.

[15] B. C. Allanach *et al.*, Eur. Phys. J. C **25**, 113 (2002).

[16] T. Hahn, Comput. Phys. Commun. **140**, 418 (2001); T. Hahn and C. Schappacher, Comput. Phys. Commun. **143**, 54 (2002).

[17] T. Hahn and M. Perez-Victoria, Comput. Phys. Commun. **118**, 153 (1999).

[18] M. Rauch, arXiv:0804.2428.

[19] M. L. Mangano, M. Moretti, and R. Pittau, Nucl. Phys. **B632**, 343 (2002).

[20] J. Alwall *et al.*, J. High Energy Phys. 09 (2007) 028; J. Alwall, P. Artoisenet, S. de Visscher, C. Duhr, R. Frederix, M. Herquet, and O. Mattelaer, AIP Conf. Proc. **1078**, 84 (2009).

[21] T. Sjostrand, S. Mrenna, and P. Skands, J. High Energy Phys. 05 (2006) 026.

[22] M. Bengtsson and T. Sjostrand, Phys. Lett. B **185**, 435 (1987); Nucl. Phys. **B289**, 810 (1987); G. Miu and T. Sjostrand, Phys. Lett. B **449**, 313 (1999); E. Norrbin and T. Sjostrand, Nucl. Phys. **B603**, 297 (2001).

[23] S. Catani, F. Krauss, R. Kuhn, and B. R. Webber, J. High Energy Phys. 11 (2001) 063; for some early work, see e.g. M. H. Seymour, Nucl. Phys. **B436**, 443 (1995); M. H. Seymour, Comput. Phys. Commun. **90**, 95 (1995).

[24] J. Alwall, S. de Visscher, and F. Maltoni, J. High Energy Phys. 02 (2009) 017; J. Alwall, K. Hiramatsu, M. M. Nojiri, and Y. Shimizu, Phys. Rev. Lett. **103**, 151802 (2009).

[25] For a new review, see e.g. W. Bernreuther, J. Phys. G **35**, 083001 (2008).

[26] S. S. D. Willenbrock, and D. A. Dicus, Phys. Rev. D **34**, 155 (1986); S. Dawson and S. S. D. Willenbrock, Nucl. Phys. **B284**, 449 (1987); D. O. Carlson and C. P. Yuan, Phys. Lett. B **306**, 386 (1993); T. Stelzer, Z. Sullivan, and S. Willenbrock, Phys. Rev. D **56**, 5919 (1997); J. M. Campbell, R. K. Ellis, and F. Tramontano, Phys. Rev. D **70**, 094012 (2004); Q. H. Cao, R. Schwienhorst, J. A. Benitez, R. Brock, and C. P. Yuan, Phys. Rev. D **72**, 094027 (2005).

[27] S. Frixione, E. Laenen, P. Motylinski, and B. R. Webber, J. High Energy Phys. 03 (2006) 092.

[28] B. W. Harris, E. Laenen, L. Phaf, Z. Sullivan, and S. Weinzierl, Phys. Rev. D **66**, 054024 (2002); Q. H. Cao, R. Schwienhorst, and C. P. Yuan, Phys. Rev. D **71**, 054023 (2005).

[29] T. M. P. Tait, Phys. Rev. D **61**, 034001 (1999); S. Zhu, arXiv:hep-ph/0109269; J. M. Campbell and F. Tramontano, Nucl. Phys. **B726**, 109 (2005); S. Frixione, E. Laenen, P. Motylinski, B. R. Webber, and C. D. White, J. High Energy Phys. 07 (2008) 029.

[30] D. O. Carlson, arXiv:hep-ph/9508278; Z. Sullivan, Phys. Rev. D **70**, 114012 (2004).

[31] R. D. Peccei, S. Peris, and X. Zhang, Nucl. Phys. **B349**, 305 (1991); T. M. P. Tait and C. P. P. Yuan, Phys. Rev. D **63**, 014018 (2000); Q. H. Cao, J. Wudka, and C. P. Yuan, Phys. Lett. B **658**, 50 (2007); J. A. Aguilar-Saavedra, Nucl. Phys. **B804**, 160 (2008).

[32] A. Heinson, A. S. Belyaev, and E. E. Boos, Phys. Rev. D **56**, 3114 (1997); T. Stelzer, Z. Sullivan, and S. Willenbrock, Phys. Rev. D **58**, 094021 (1998); A. S. Belyaev, E. E. Boos, and L. V. Dudko, Phys. Rev. D **59**, 075001 (1999).

[33] As the expert reader will observe at the end of the discussion, there is no reason why equivalent results could not be obtained using the MC@NLO generator for the single top channels [27]. However, direct top production is not available in the same framework yet.

[34] F. Maltoni, Z. Sullivan, and S. Willenbrock, Phys. Rev. D **67**, 093005 (2003); E. Boos and T. Plehn, Phys. Rev. D **69**, 094005 (2004); J. M. Campbell, R. Frederix, F. Maltoni, and F. Tramontano, Phys. Rev. Lett. **102**, 182003 (2009).

[35] G. Mahlon and S. J. Parke, Phys. Lett. B **476**, 323 (2000); Z. Sullivan, Phys. Rev. D **72**, 094034 (2005); G. Mahlon, arXiv:hep-ph/0011349; P. Motylinski, Phys. Rev. D **80**, 074015 (2009).